Isospin- and momentum-dependent effective interactions for the baryon octet and the properties of hybrid stars

Jun Xu,[1] Lie-Wen Chen,[2,3] Che Ming Ko,[4] and Bao-An Li[5]

[1]*Cyclotron Institute, Texas A&M University, College Station, Texas 77843-3366, USA*

[2]*Department of Physics, Shanghai Jiao Tong University, Shanghai 200240, China*

[3]*Center of Theoretical Nuclear Physics, National Laboratory of Heavy Ion Accelerator, Lanzhou 730000, China*

[4]*Cyclotron Institute and Department of Physics and Astronomy, Texas A&M University, College Station, Texas 77843-3366, USA*

[5]*Department of Physics and Astronomy, Texas A&M University-Commerce, Commerce, Texas 75429-3011, USA*

(Received 11 January 2010; published 20 May 2010)

The isospin- and momentum-dependent MDI interaction, which has been extensively used in intermediate-energy heavy-ion reactions to study the properties of asymmetric nuclear matter, is extended to include the nucleon-hyperon and hyperon-hyperon interactions by assuming the same density, momentum, and isospin dependence as for the nucleon-nucleon interaction. The parameters in these interactions are determined from the empirical hyperon single-particle potentials in symmetric nuclear matter at saturation density. The extended MDI interaction is then used to study in the mean-field approximation the equation of state of hypernuclear matter and also the properties of hybrid stars by including the phase transition from hypernuclear matter to quark matter at high densities. In particular, the effects of attractive and repulsive ΣN interactions and different values of symmetry energies on the hybrid star properties are investigated.

DOI: 10.1103/PhysRevC.81.055803 PACS number(s): 21.65.−f, 21.30.Fe, 26.60.−c, 97.60.Jd

I. INTRODUCTION

The study of in-medium baryon-baryon effective interactions is one of the fundamental problems in nuclear physics. Although significant progress has been made in understanding the nucleon-nucleon interaction in the nuclear medium, our knowledge of hyperon-nucleon and hyperon-hyperon interactions in the nuclear medium is very limited. The latter is important for understanding the properties of hypernuclei, the equation of state (EOS) of dense baryonic matter, the properties of compact stars in which hyperons are expected to appear abundantly, and strangeness production in heavy-ion collisions. Therefore, it is of great interest to develop an effective model for hyperon-nucleon and hyperon-hyperon interactions in the nuclear medium.

The in-medium single-particle potential of a nucleon generally depends not only on the nuclear density and its momentum but also on its isospin. The isospin- and momentum-dependent (MDI) interaction is such an effective nuclear interaction based on the finite-range Gogny interaction [1]. This interaction has recently been extensively used in studying the isospin- and momentum-dependent effects in nuclear reactions and the properties of neutron stars (for a recent review see Ref. [2]). In particular, by using this interaction in the isospin-dependent Boltzmann-Uheling-Ulenback (IBUU) transport model with isospin-dependent in-medium nucleon-nucleon scattering cross sections, a relatively stringent constraint on the density dependence of the nuclear symmetry energy at subsaturation densities was obtained from the isospin diffusion data in intermediate-energy heavy-ion collisions [3–5]. The resulting symmetry energy has been used to constrain the neutron skin thickness of heavy nuclei [6] and the properties of neutron stars [7–11] including the transition density, which separates the liquid core from the inner crust of a neutron star, and other properties of neutron stars by assuming that they only consist of nucleons, electrons, and muons [12,13].

In this paper, we extend the MDI interaction to include nucleon-hyperon and hyperon-hyperon interactions. This is achieved by assuming that the nucleon-hyperon and hyperon-hyperon interactions have the same density and momentum dependence as the nucleon-nucleon interaction with the interaction parameters fitted to known experimental data at normal nuclear matter density. With this extended MDI interaction, we then study, as an example, the properties of hybrid stars that consist not only of an appreciable fraction of hyperons but also possible quark matter in their dense core [14–26]. For the hadron-quark phase transition, we use the Gibbs construction [27,28] with the quark phase described by a simple MIT bag model [16,29]. In particular, we study the effects of attractive and repulsive ΣN interactions and different symmetry energies on the properties of hybrid stars. We note that there have been extensive studies on hybrid stars based on various approaches, such as the relativistic mean-field (RMF) model [30–34], Brueckner-Hartree-Fock theroy [35–39], and phenomenological models [40,41].

This paper is organized as follows. In Sec. II, we describe the method used in extending the MDI interaction to include the hyperon-nucleon and hyperon-hyperon interactions. The extended MDI interaction is then used in Sec. III A to study the thermodynamical properties of hypernuclear matter and its equilibrium conditions. The MIT bag model is used in Sec. III B to describe the properties of the quark matter and in Sec. III C to study the hadron-quark phase transition in dense matter. In Sec. IV, we show and discuss the results on the particle fractions in dense matter and its equation of state as well as the mass-radius relation of hybrid stars in different scenarios. A summary is given in Sec. V.

II. THE MDI INTERACTION WITH HYPERONS

The MDI interaction is an effective nuclear interaction with its density and momentum dependence deduced from

the phenomenological finite-range Gogny interaction [1]. In the mean-field approximation, the potential energy density in nuclear matter of density ρ and isospin asymmetry $\delta = (\rho_n - \rho_p)/\rho$ with ρ_n and ρ_p being, respectively, the neutron and proton densities, is given by

$$V(\rho,\delta) = \frac{A_u(x)\rho_n\rho_p}{\rho_0} + \frac{A_l(x)}{2\rho_0}\left(\rho_n^2+\rho_p^2\right) + \frac{B}{\sigma+1}\frac{\rho^{\sigma+1}}{\rho_0^\sigma} \times (1-x\delta^2) + \frac{1}{\rho_0}\sum_{\tau,\tau'} C_{\tau,\tau'} \times \iint d^3p d^3p' \frac{f_\tau(\vec{r},\vec{p}) f_{\tau'}(\vec{r},\vec{p}')}{1+(\vec{p}-\vec{p}')^2/\Lambda^2}, \quad (1)$$

where $\tau(\tau')$ is the nucleon isospin, $f_\tau(\vec{r},\vec{p})$ is the nucleon phase distribution function, and $\rho_0 = 0.16\ \mathrm{fm}^{-3}$ is the saturation density of normal nuclear matter. Values of the parameters $A_u(x), A_l(x), B, \sigma, \Lambda, C_l = C_{\tau,\tau}$ and $C_u = C_{\tau,-\tau}$ can be found in Refs. [1,4]. The parameter x, related to the coefficient of the spin-exchange operator in the Gogny-Skyrme interactions, is used to adjust the density dependence of the symmetry energy away from the saturation density without changing the properties of symmetric nuclear matter. At subsaturation densities, its value has been constrained between 0 and -1 from the analysis of the isospin-diffusion and neutron-skin-thickness data [3–5,42].

A. The extended MDI interaction

To extend the MDI interaction for the nucleon-nucleon (NN) interaction to include the nucleon-hyperon (NY) and hyperon-hyperon (YY) interactions, we assume that the latter have the same density and momentum dependence as that between two nucleons. The potential energy density of a hypernuclear matter resulting from interactions between any two baryons then has the following general form:

$$V_{bb'} = \sum_{\tau_b,\tau'_{b'}}\left[\frac{A_{bb'}}{2\rho_0}\rho_{\tau_b}\rho_{\tau'_{b'}} + \frac{A'_{bb'}}{2\rho_0}\tau_b\tau_{b'}\rho_{\tau_b}\rho_{\tau'_{b'}} + \frac{B_{bb'}}{\sigma+1}\frac{\rho^{\sigma-1}}{\rho_0^\sigma}\left(\rho_{\tau_b}\rho_{\tau'_{b'}} - x\tau_b\tau_{b'}\rho_{\tau_b}\rho_{\tau'_{b'}}\right) + \frac{C_{\tau_b,\tau'_{b'}}}{\rho_0}\iint d^3p d^3p' \frac{f_{\tau_b}(\vec{r},\vec{p}) f_{\tau'_{b'}}(\vec{r},\vec{p}')}{1+(\vec{p}-\vec{p}')^2/\Lambda^2}\right], \quad (2)$$

where b (b') denotes the baryon octet included in the present study,(i.e., N, Λ, Σ, and Ξ). We use the conventions that $\tau_N = -1$ for the neutron and 1 for the proton [43]; $\tau_\Lambda = 0$ for the Λ; $\tau_\Sigma = -1$ for the Σ^-, 0 for the Σ^0, and 1 for the Σ^+; and $\tau_\Xi = -1$ for the Ξ^- and 1 for the Ξ^0. Here, the total baryon density is now given by $\rho = \sum_b \sum_{\tau_b}\rho_{\tau_b}$, and $f_{\tau_b}(\vec{r},\vec{p})$ is the phase-space distribution function of particle species τ_b. The interaction parameters are denoted by $A_{bb'}$, $A'_{bb'}$, $B_{bb'}$, and C_{τ_b,τ'_b}. If there are only nucleons, we can rewrite $A_{NN} = (A_l + A_u)/2$, $A'_{NN} = (A_l - A_u)/2$, $B_{NN} = B$, and $C_{\tau_N,\tau'_N} = C_l$ for $\tau_N = \tau'_N$ and $= C_u$ for $\tau_N \neq \tau'_N$, which then reduce to the original parameters in the MDI interaction for nucleons [1,4]. The parameter x is again used to model the isospin effect on the interaction between two baryons, and its value is taken to be 0 or -1 in the present study for all baryon pairs.

The single-particle potential for a baryon of species τ_b in hypernuclear matter can then be obtained from the total potential energy density of the hypernuclear matter, given by $V_{HP} = (1/2)\sum_{b,b'} V_{bb'}$, as

$$\begin{aligned} U_{\tau_b}(p) &= \frac{\delta}{\delta\rho_{\tau_b}} V_{HP} \\ &= \sum_{b'(b'\neq b)}\sum_{\tau'_{b'}}\left[\frac{A_{bb'}}{2\rho_0}\rho_{\tau'_{b'}} + \frac{A'_{bb'}}{2\rho_0}\tau_b\tau'_{b'}\rho_{\tau'_{b'}} + \frac{B_{bb'}}{\sigma+1}\frac{\rho^{\sigma-1}}{\rho_0^\sigma}\left(\rho_{\tau'_{b'}} - x\tau_b\tau'_{b'}\rho_{\tau'_{b'}}\right) + \frac{C_{\tau_b,\tau'_{b'}}}{\rho_0}\int d^3p' \frac{f_{\tau'_{b'}}(\vec{r},\vec{p}')}{1+(\vec{p}-\vec{p}')^2/\Lambda^2}\right] \\ &\quad + \sum_{\tau'_b}\left[\frac{A_{bb}}{\rho_0}\rho_{\tau'_b} + \frac{A'_{bb}}{\rho_0}\tau_b\tau'_b\rho_{\tau'_b} + \frac{2B_{bb}}{\sigma+1}\frac{\rho^{\sigma-1}}{\rho_0^\sigma}\left(\rho_{\tau'_b} - x\tau_b\tau'_b\rho_{\tau'_b}\right) + \frac{2C_{\tau_b,\tau'_b}}{\rho_0}\int d^3p' \frac{f_{\tau'_b}(\vec{r},\vec{p}')}{1+(\vec{p}-\vec{p}')^2/\Lambda^2}\right] \\ &\quad + \sum_{b',b''}\left[B_{b'b''}\frac{\sigma-1}{\sigma+1}\frac{\rho^{\sigma-2}}{\rho_0^\sigma}\sum_{\tau_{b'}}\sum_{\tau'_{b''}}\left(\rho_{\tau_{b'}}\rho_{\tau'_{b''}} - x\tau_{b'}\tau'_{b''}\rho_{\tau_{b'}}\rho_{\tau'_{b''}}\right)\right]. \end{aligned} \quad (3)$$

For the interaction parameters $A_{bb'}$, $A'_{bb'}$, $B_{bb'}$, and $C_{\tau_b,\tau'_{b'}}$ that involve hyperons, they can in principle be determined from the nucleon-hyperon and hyperon-hyperon interactions in free space. Because of the lack of hyperon-nucleon scattering experiments, information on the hyperon-nucleon interactions has been mainly obtained from the hyperon single-particle potentials extracted empirically from studying Λ [44] as well as Σ [45,46] and Ξ [47] production in nuclear reactions. Although this has led to extensive studies of the hyperon-nucleon interaction in the past [48–50], the isospin and momentum dependence of the hyperon-nucleon in-medium interactions is still not very well determined, and the situation is even worse for hyperon-hyperon interactions. We therefore assume in the present study that $A_{bb'}$, $A'_{bb'}$, $B_{bb'}$, and $C_{\tau_b,\tau'_{b'}}$ are all proportional to corresponding ones in the nucleon-nucleon interaction. Specifically, for $A_{bb'}$, $A'_{bb'}$, and $B_{bb'}$,

TABLE I. Parameters for the MDI-Hyp-A and MDI-Hyp-R interactions with $x = 0$ and $x = -1$. All parameters except σ are in units of MeV. $A'_{N\Sigma}$(A) and $B_{N\Sigma}$(A) are for the MDI-Hyp-A interaction, and $A'_{N\Sigma}$(R) and $B_{N\Sigma}$(R) are for the MDI-Hyp-R interaction. Other parameters are the same for both interactions.

A_{NN}	$A_{N\Lambda}$	$A_{N\Sigma}$	$A_{N\Xi}$	$A_{\Lambda\Lambda}$	$A_{\Lambda\Sigma}$	$A_{\Lambda\Xi}$	$A_{\Sigma\Sigma}$	$A_{\Sigma\Xi}$	$A_{\Xi\Xi}$	Λ	σ
−108.28	−108.28	−108.28	−79.04	−68.21	−135.34	−135.34	−53.05	−108.28	−57.39	263.04	4/3
x	A'_{NN}	$A'_{N\Sigma}$(A)	$A'_{N\Sigma}$(R)	$A'_{N\Xi}$	$A'_{\Sigma\Sigma}$	$A'_{\Sigma\Xi}$	$A'_{\Xi\Xi}$				
0	−12.29	−12.29	−28.65	−8.98	−6.02	−12.29	−6.52				
−1	−103.45	−103.45	−241.04	−75.52	−50.69	−103.45	−54.83				
B_{NN}	$B_{N\Lambda}$	$B_{N\Sigma}$(A)	$B_{N\Sigma}$(R)	$B_{N\Xi}$	$B_{\Lambda\Lambda}$	$B_{\Lambda\Sigma}$	$B_{\Lambda\Xi}$	$B_{\Sigma\Sigma}$	$B_{\Sigma\Xi}$	$B_{\Xi\Xi}$	
106.35	106.35	106.35	247.80	77.64	67.00	132.94	132.94	52.11	106.35	56.37	
C_{τ_N,τ_N}	$C_{\tau_N,-\tau_N}$	C_{τ_N,τ_Σ}	$C_{\tau_N,-\tau_\Sigma}$	C_{τ_N,τ_Ξ}	$C_{\tau_N,-\tau_\Xi}$	$C_{\tau_\Sigma,\tau_\Sigma}$	$C_{\tau_\Sigma,-\tau_\Sigma}$	C_{τ_Σ,τ_Ξ}	$C_{\tau_\Sigma,-\tau_\Xi}$	C_{τ_Ξ,τ_Ξ}	$C_{\tau_\Xi,-\tau_\Xi}$
−11.70	−103.40	−11.70	−103.40	−8.54	−75.48	−5.73	−50.67	−11.70	−103.40	−6.20	−54.80
$C_{N\Lambda}$	$C_{N\Sigma^0}$	$C_{\Lambda\Lambda}$	$C_{\Lambda\Sigma}$	$C_{\Lambda\Xi}$	$C_{\Sigma^0\Sigma}$	$C_{\Sigma^0\Xi}$					
−57.55	−57.55	−36.26	−71.94	−71.94	−28.20	−57.55					

we assume

$$\begin{aligned} A_{bb'} &= f_{bb'} A_{NN}, \\ A'_{bb'} &= f_{bb'} A'_{NN}, \\ B_{bb'} &= f_{bb'} B_{NN}, \end{aligned} \tag{4}$$

and for $C_{\tau_b,\tau'_{b'}}$ we assume

$$C_{\tau_b,\tau'_{b'}} = \begin{cases} f_{bb'} \frac{C_l + C_u}{2} & (\tau_b \text{ or } \tau'_{b'} = 0), \\ f_{bb'} C_l & (\tau_b = \tau'_{b'} \neq 0), \\ f_{bb'} C_u & (\tau_b \neq \tau'_{b'} \neq 0), \end{cases}$$

with Λ and Σ^0 treated differently.

We determine the values of $f_{bb'}$ by fitting the empirical potential $U_b^{(b')}$ of baryon b at rest in a medium consisting of baryon species b'. For hyperons in symmetric nuclear matter at saturation density, their potentials are

$$U_\Lambda^{(N)}(\rho_N = \rho_0) = -30 \text{ MeV} \tag{5}$$

for the Λ potential from the analysis of (π^+, K^+) and (K^-, π^-) reactions on nuclei [51,52] and

$$U_\Xi^{(N)}(\rho_N = \rho_0) = -18 \text{ MeV} \tag{6}$$

for the Ξ potential from the analysis of $(\Xi, {}^4_\Lambda H)$ [53] and (K^-, K^+) [54,55] reactions. This leads to the values $f_{N\Lambda} = 1$ and $f_{N\Xi} = 0.73$. For the Σ hyperon, its potential was taken to be attractive in earlier studies [45], but more recent analyses indicate that it is repulsive in the nuclear medium [56–60]. In the present work, we consider both the attractive and repulsive cases

$$U_\Sigma^{(N)}(\rho_N = \rho_0) = \pm 30 \text{ MeV}. \tag{7}$$

By setting $f_{N\Sigma} = 1$ we get an attractive ΣN interaction, and this is called MDI-Hyp-A in the following. To obtain a repulsive ΣN interaction, called MDI-Hyp-R in the following, we adjust the values of positive and negative terms in the single-particle potential by setting $B_{N\Sigma} = 2.33 B_{NN}$ and $A'_{N\Sigma} = 2.33 A'_{NN}$ without changing other parameters as in the case of the MDI-Hyp-A interaction. A similar method of changing an attractive ΣN interaction to a repulsive one was used in the RMF calculation [31] by changing the coupling constants of ω and ρ mesons. For the hyperon-hyperon interaction, the parameters are fitted according to [61]

$$U_Y^{(Y')}(\rho_{Y'} = \rho_0) \sim -40 \text{ MeV}, \tag{8}$$

which gives the strength of the hyperon-hyperon interactions as $f_{\Lambda\Lambda} = 0.63$, $f_{\Lambda\Sigma} = 1.25$, $f_{\Lambda\Xi} = 1.25$, $f_{\Sigma\Sigma} = 0.49$, $f_{\Sigma\Xi} = 1$, and $f_{\Xi\Xi} = 0.53$. Detailed values of the parameters are listed in Table I. These parametrizations can be viewed as a baseline for studying the properties of hypernuclear matter, and more sophisticated treatments are left for future work after the in-medium properties of hyperons are better understood. It will be shown in the following that many interesting results can already be obtained even with these simple parametrizations.

B. Single-particle potentials

An important quantity related to the interaction of a particle in the nuclear medium is its single-particle potential as given by Eq. (3), which is also needed later in our study of the properties of neutron stars. The single-particle potential of a particle depends not only on the density of the medium but also on the momentum of the particle. In this section, we show and discuss the single-particle potentials of both nucleons and hyperons in nuclear matter obtained from the extended MDI interaction.

We first show in Fig. 1 the single-particle potential of a particle at rest in symmetric nuclear matter as a function of density. Although the nucleon potential is more attractive at normal density than those of hyperons, it becomes more repulsive than the hyperon potentials above about five times normal nuclear density, including the Σ potential that is attractive at normal density. For the Σ potential that is repulsive at normal density, it becomes more repulsive as the density increases and becomes slightly attractive only at very low densities. Comparing our results with those from other models given in Ref. [62] (and references therein), we see that the single-particle potentials of Λ and Σ are close to those from the chiral effective field theory [63], but they are more repulsive than those based on the G-matrix calculations using the soft-core Nijmegen model or the Jülich meson-exchange

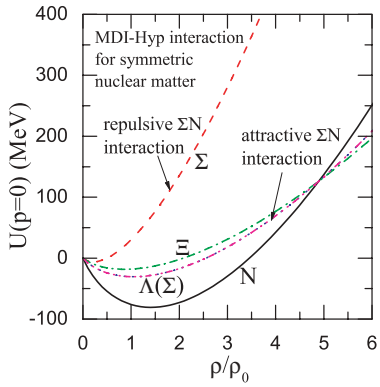

FIG. 1. (Color online) Single-particle potentials for particles at rest in symmetric nuclear matter as functions of density.

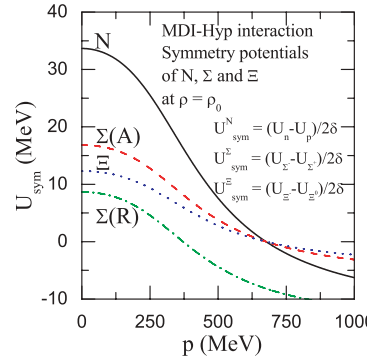

FIG. 3. (Color online) Symmetry potentials of nucleons and Σ and Ξ hyperons in asymmetric nuclear matter at saturation density $\rho = \rho_0$. Σ(A) and Σ(R) are for the MDI-Hyp-A and MDI-Hyp-R interactions, respectively.

model for the free hyperon-nucleon interactions, particularly at high densities.

The single-particle potential of a particle from the extended MDI interaction also depends on its momentum. Figure 2 shows the momentum dependence of the single-particle potentials for both nucleons and hyperons in symmetric nuclear matter at saturation density. Again, results using both attractive and repulsive ΣN interactions (i.e., MDI-Hyp-A and MDI-Hyp-R) are shown for comparison. Also indicated in the figure is the Fermi momentum of nucleons. For nucleons, the single-particle potential from the MDI interaction is consistent with the Schrödinger equivalent potential obtained by Hama and co-workers from nucleon-nucleus scattering data [64,65] up to nucleon momentum of 500 MeV. For hyperons, the momentum dependence of their single-particle potentials from the extended MDI interaction is similar to that obtained from the G-matrix calculations based on the free Nijmegen NY interaction [37]. Both show an increase with increasing momentum and are similar at low momenta as both are constrained by available experimental data. They are, however, slightly different at high momenta. The momentum dependence of NY and YY interactions thus remains an

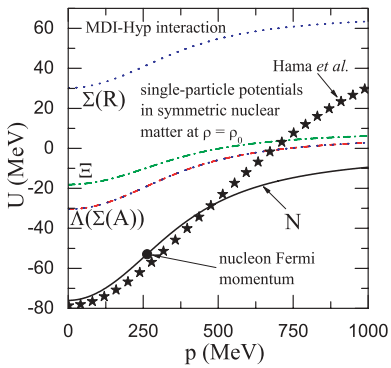

FIG. 2. (Color online) Single-particle potentials in symmetric nuclear matter at saturation density ρ_0 as functions of particle momentum. The Schrödinger equivalent potential obtained by Hama and co-workers [64,65] from the nucleon-nucleus scattering data is shown by stars for comparison. Σ(A) and Σ(R) are for the MDI-Hyp-A and MDI-Hyp-R interactions, respectively.

open question, especially at high momenta. Also, the density dependence of the high-momentum behavior of the mean-field potential is poorly known. Since the maximum Fermi momenta of nucleons and hyperons reached in hybrid stars are not very high, the incorrect nucleon potential and the uncertainty of hyperon potentials at high momenta given by the extended MDI interaction are thus not expected to affect significantly the properties of cold hypernuclear matter considered in the present study.

It is known that both proton and neutron single-particle potentials in asymmetric nuclear matter of unequal proton and neutron densities are approximately linear in the isospin asymmetry δ of the matter. Whether this is also the case for hyperons is not clear in the literature. For the extended MDI interaction introduced in the present study, such a linear dependence on isospin asymmetry, however, also holds for Σ and Ξ hyperons. The single-particle potential of a particle in asymmetric nuclear matter can thus be written in general as $U_{\tau_b}(\rho,\delta) \approx U_{\tau_b}(\rho,\delta=0) - \tau_b U^b_{\rm sym}(\rho)\delta$ in terms of the symmetry potential $U^b_{\rm sym}(\rho)$, defined by $U^N_{\rm sym}(\rho) = [U_n(\rho,\delta) - U_p(\rho,\delta)]/2\delta$, $U^\Sigma_{\rm sym}(\rho) = [U_{\Sigma^-}(\rho,\delta) - U_{\Sigma^+}(\rho,\delta)]/2\delta$, and $U^\Xi_{\rm sym}(\rho) = [U_{\Xi^-}(\rho,\delta) - U_{\Xi^0}(\rho,\delta)]/2\delta$ for the nucleon and Σ and Ξ hyperons, respectively. From the single-particle potentials of nucleons and Σ and Ξ hyperons in asymmetric nuclear matter at normal nuclear matter density and of isospin asymmetry $\delta = 0.2$, we have calculated their symmetry potentials using these definitions. In Fig. 3, the momentum dependence of these symmetry potentials are compared. All symmetry potentials are seen to decrease with increasing momentum. At zero momentum, the symmetry potentials of the nucleon and the Ξ are about 34 and 12 MeV, respectively, and for the Σ hyperon they are 17 MeV for an attractive ΣN interaction and 9 MeV for a repulsive one.

Although the symmetry potentials at normal nuclear density are independent of the value of x, which is used in the MDI interaction to model the stiffness of nuclear symmetry energy at densities different from the normal density, this is not the case at other densities. This is demonstrated in Fig. 4 for the symmetry potentials of the nucleon and the Σ hyperon and the Ξ hyperon in asymmetric nuclear matter at density $\rho = 3\rho_0$

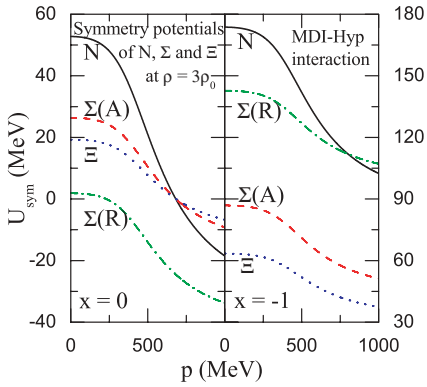

FIG. 4. (Color online) Symmetry potentials of nucleons and Σ and Ξ hyperons in asymmetric nuclear matter at density $\rho = 3\rho_0$. Σ(A) and Σ(R) are for the MDI-Hyp-A and MDI-Hyp-R interactions, respectively. Note that different scales are used for $x = 0$ (left panel) and $x = -1$ (right panel).

for the two symmetry energy parameters $x = 0$ and $x = -1$. For $x = 0$, the symmetry potentials at zero momentum are 53 and 19 MeV for the nucleon and the Ξ hyperon, respectively, and for the Σ hyperon they are 26 MeV with the MDI-Hyp-A interaction and 2 MeV with the MDI-Hyp-R interaction. These values are changed to 174 and 63 MeV for the nucleon and the Ξ hyperon, respectively, and for the Σ hyperon to 87 MeV for the MDI-Hyp-A interaction and 143 MeV for the MDI-Hyp-R interaction for the case of $x = -1$. As noted in Ref. [66], the charged Σ baryon ratio in heavy-ion collisions can be used as a probe to constrain the nuclear symmetry energy (potential) at densities larger than $3\rho_0$. It will be very interesting to see how the symmetry potentials of Σ and Ξ hyperons in nuclear matter affect the charged Σ hyperon ratio and the charged Ξ hyperon ratio in heavy-ion collisions induced by neutron-rich nuclei. This is important for determining the high-density behavior of the nuclear symmetry energy using these ratios in heavy-ion collisions. The extended MDI interaction with hyperons is therefore useful for studying the nuclear symmetry energy (potential) at $\rho > 3\rho_0$ in the transport model calculation for heavy-ion collisions.

III. EQUILIBRIUM CONDITIONS AND THERMODYNAMICAL RELATIONS IN DENSE MATTER

The extended MDI interaction is also useful for studying the properties of a hybrid star that is expected to have a quark core at high densities, a mixed phase of quarks and hadrons at moderate densities, and a hadron phase at low densities. We review in this section the β-equilibrium, charge neutrality, and baryon number conservation conditions of such matter.

A. The hadron phase

In the hadron phase of a hybrid star, the matter consists of nucleons, hyperons, and leptons. For leptons, we include both electrons and muons with their masses taken to be 0 and 106 MeV, respectively. At equilibrium, these particles satisfy following baryon number conservation, charge neutrality, and β-equilibrium conditions:

$$\sum_i \rho_i b_i = \rho, \tag{9}$$

$$\sum_i \rho_i q_i = 0, \tag{10}$$

$$\mu_i = \mu_b^H b_i - \mu_c^H q_i. \tag{11}$$

Here, q_i and b_i are, respectively, the charge and baryon numbers of particle species i, where i can be nucleons, hyperons, or leptons, and their density and chemical potential are denoted, respectively, by ρ_i and μ_i. The total baryon density of the hadron phase is denoted by ρ, and μ_b^H and μ_c^H are, respectively, the baryon and charge chemical potentials of the hadron phase.

By taking into account their interactions in the mean-field approximation, the chemical potential of baryon species τ_b is given by

$$\mu_{\tau_b}(p_{F\tau_b}) = m_{\tau_b} + \frac{p_{F\tau_b}^2}{2m_{\tau_b}} + U_{\tau_b}(p_{F\tau_b}), \tag{12}$$

where $p_{F\tau_b}$ is their Fermi momentum, and U_{τ_b} and m_{τ_b} are, respectively, the single-particle potential and mass of the baryon. For leptons ($l = \mu, e$) their chemical potential is given by $\mu_l = (m_l^2 + p_{Fl}^2)^{1/2}$ with $p_{Fl} = (3\pi^2\rho_l)^{1/3}$ being their Fermi momentum. The relative abundances of various hadrons and leptons for a given total baryon density are then obtained by solving these equations.

In terms of the densities of various particles, the total energy density of the hadron phase can be written as

$$\epsilon^H = V_H + V_L, \tag{13}$$

where V_H and V_L are the contributions from baryons and leptons, respectively. The former can be written as

$$V_H = V_{HP} + V_{HK} + V_{HM}, \tag{14}$$

where $V_{HP} = (1/2)\sum_{b,b'} V_{bb'}$ is the potential energy density of baryons with $V_{bb'}$ calculated from Eq. (2), and V_{HK} and V_{HM} are, respectively, the kinetic energy and mass contributions given by

$$V_{HK} = \sum_b \sum_{\tau_b} \frac{p_{F\tau_b}^5}{10\pi^2 m_{\tau_b}}, \tag{15}$$

$$V_{HM} = \sum_b \sum_{\tau_b} \rho_{\tau_b} m_{\tau_b}. \tag{16}$$

The contribution V_L from leptons is calculated by treating them as a free Fermi gas, that is,

$$V_L = V_e + V_\mu,$$

$$V_e = \frac{p_{Fe}^4}{4\pi^2},$$

$$V_\mu = \frac{1}{4\pi^2}\left[p_{F\mu}\mu_\mu^3 - \frac{1}{2}m_\mu^2 p_{F\mu}\mu_\mu - \frac{1}{2}m_\mu^4 \ln\left(\frac{p_{F\mu}+\mu_\mu}{m_\mu}\right)\right]. \tag{17}$$

The pressure of the hadron phase is obtained from the thermodynamical relation

$$P^H = P_H + P_L = \left(\sum_b \sum_{\tau_b} \mu_{\tau_b}\rho_{\tau_b} - V_H\right) + \left(\sum_l \mu_l\rho_l - V_L\right), \quad (18)$$

where b and l run over all species of baryons and leptons, respectively. We note that the thermodynamical consistency condition

$$P^H = \rho^2 \frac{d(\epsilon^H/\rho)}{d\rho} \quad (19)$$

is satisfied.

B. The quark phase

As the nuclear matter density increases, such as in the core of neutron stars, not only do hyperons appear but also quark matter could exist [15]. To take into consideration possible transition between the hadronic matter and the quark matter, we follow many previous studies to use in the present study the MIT bag model [16,29] to describe the cold quark matter that might exist in the dense core of neutron stars.

For the quark phase consisting of quarks and leptons, the baryon number conservation and charge neutrality conditions are given by expressions similar to Eqs. (9) and (10) with i denoting now quarks and leptons. For the β-equilibrium condition in the quark phase, it is given by $\mu_i = \mu_b^Q b_i - \mu_c^Q q_i$ with μ_b^Q and μ_c^Q being the baryon and charge chemical potentials of the quark phase, respectively.

The total energy density and pressure of the quark phase can be calculated from

$$\epsilon^Q = V_Q + V_L, \quad (20)$$

$$P^Q = P_Q + P_L, \quad (21)$$

where V_Q and P_Q are the energy density and pressure of quarks, which can be calculated from the MIT bag model as described in the following, and V_L and P_L are the energy density and pressure of leptons given by the same expressions as those in the hadron phase.

At zero temperature, the density ρ_f, chemical potential μ_f, and energy density V_f of quarks of flavor $f = u, d, s$ in the quark matter are given, respectively, by

$$\rho_f = \frac{p_{Ff}^3}{\pi^2},$$
$$\mu_f = \sqrt{m_f^2 + p_{Ff}^2},$$
$$V_f = \frac{3}{4\pi^2}\left[p_{Ff}\mu_f^3 - \frac{1}{2}m_f^2 p_{Ff}\mu_f - \frac{1}{2}m_f^4 \ln\left(\frac{p_{Ff}+\mu_f}{m_f}\right)\right], \quad (22)$$

where p_{Ff} is the Fermi momentum of quarks of flavor f. For the quark masses, they are taken to be $m_u = m_d = 0$ and $m_s = 150$ MeV. In the bag model, the energy density is modified by a bag constant B, resulting in an energy density given by

$$V_Q = \sum_f V_f + B. \quad (23)$$

This leads to the following pressure for the quark matter:

$$P_Q = \sum_f \mu_f\rho_f - V_Q = \rho^2 \frac{d(V_Q/\rho)}{d\rho}, \quad (24)$$

where ρ is the total baryon density of the quark phase,

$$\rho = \frac{1}{3}\sum_f \rho_f. \quad (25)$$

C. The hadron-quark phase transition

The hadron-quark phase transition leads to a mixed phase of hadronic and quark matter, which is usually described by the Gibbs conditions [27,28]

$$T^H = T^Q, \qquad P^H = P^Q,$$
$$\mu_b = \mu_b^H = \mu_b^Q, \qquad \mu_c = \mu_c^H = \mu_c^Q. \quad (26)$$

The Gibbs conditions for the chemical potentials can also be expressed as

$$\mu_u = \tfrac{1}{3}\mu_n - \tfrac{2}{3}\mu_e,$$
$$\mu_d = \mu_s = \tfrac{1}{3}\mu_n + \tfrac{1}{3}\mu_e. \quad (27)$$

Since only the case of zero temperature is considered in this paper, the first condition in Eq. (26) is always satisfied. To solve these equations, we follow the method of Ref. [28]. In this method, one first calculates the pressure of the hadron phase at a series of baryon densities. From the known chemical potentials μ_n and μ_e of hadronic matter at these densities, one then calculates the pressure of the quark matter that is in chemical equilibrium with corresponding hadronic matter, that is, with the quark chemical potentials μ_u, μ_d, and μ_s determined by the two relations in Eq. (27). The hadronic baryon density at which the two pressures are the same is then the low-density boundary of the hadron-quark phase transition. As an illustration, we show in Fig. 5 the results for the case of the symmetry energy parameter $x = 0$ and the bag constant $B^{1/4} = 180$ MeV. The solid line is the density dependence of the pressure of the hadron phase calculated using the model described in Sec. III A; the dash-dotted line is the pressure of the quark matter that is in chemical equilibrium with the hadronic matter as a function of the baryon density of the hadronic matter. The low-density boundary of the hadron-quark phase transition is indicated by the intersection of the solid line and the dash-dotted line.

Above this low-density boundary, the dense matter enters the mixed phase, in which the hadron phase and the quark phase satisfy following chemical equilibrium, mechanical equilibrium, baryon number conservation, and charge neutrality conditions:

$$\mu_b b_i - \mu_c q_i = \mu_i,$$
$$P^H = P^Q,$$

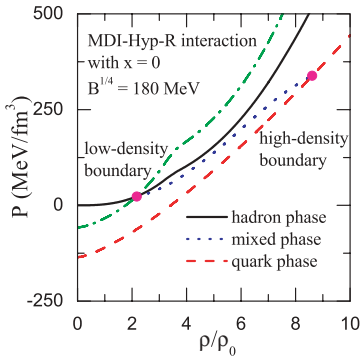

FIG. 5. (Color online) Pressure as functions of baryon density ρ for the hadron phase (solid line), mixed phase (dotted line), and quark phase (dashed line). The pressure of the quark matter that is in chemical equilibrium with the hadronic matter as a function of the baryon density of the hadronic matter is denoted by the dash-dotted line, whose intersection with the solid line gives the low-density boundary of the hadron-quark phase transition.

$$(1-Y)\sum_b\sum_{\tau_b}\rho_{\tau_b}+\frac{Y}{3}\sum_f\rho_f=\rho,$$
$$(1-Y)\sum_b\sum_{\tau_b}\rho_{\tau_b}q_{\tau_b}+\frac{Y}{3}\sum_f\rho_f q_f+\sum_l\rho_l q_l=0, \quad (28)$$

where i runs over baryons, leptons, and quarks, and Y is the baryon number fraction of the quark phase. We note that in the mixed phase the total charge is zero and the leptons play an important role in maintaining the charge neutrality and β-equilibrium conditions. The total energy density and pressure of the mixed phase are calculated according to

$$\epsilon^M=(1-Y)V_H+YV_Q+V_L,$$
$$P^M=(1-Y)P_H+YP_Q+P_L. \quad (29)$$

It is obvious that we have a pure hadron phase for $Y=0$ and a pure quark phase for $Y=1$. For the case of the symmetry energy parameter $x=0$ and the bag constant $B^{1/4}=180$ MeV considered here, the pressure of the mixed phase as a function of the baryon density obtained from solving Eq. (28) is shown in Fig. 5 by the dotted line. The mixed phase starts at the low-density boundary of the hadron-quark phase transition and ends at the high-density boundary of the hadron-quark phase transition when the matter is purely quark matter, whose pressure is calculated using the model described in Sec. III B and is shown by the dashed line in Fig. 5 as a function of the baryon density.

There is a recent study based on the relativistic mean-field model for the hadron phase and the MIT bag model for the quark phase to compare the behavior of the mixed phase in the Gibbs construction with that in the Maxwell construction, which does not require the same charge chemical potential for the hadronic matter and quark matter in the mixed phase [67]. The pressure of the mixed phase in the Maxwell construction is found to be constant with respect to its baryon density, which is in contrast with the increasing pressure of the mixed phase with increasing baryon density in the Gibbs construction as seen in Fig. 5. It is worthwhile to point out that although the charge neutrality condition in Eq. (28) is satisfied globally, it is violated in each phase. A more realistic equation of state of the mixed phase can be obtained from the Wigner-Seitz cell calculation by taking into account Coulomb and surface effects. The equation of state of the mixed phase obtained from this approach lies between those from the Gibbs and Maxwell constructions. The latter can thus be viewed as two extreme cases corresponding to certain values of the surface tension parameter in the Wigner-Seitz cell calculation [68,69].

IV. RESULTS AND DISCUSSION

In this section, we use the extended MDI (MDI-Hyp) interaction to study the equation of state and the relative particle fractions in charge-neutral and β-stable hypernuclear matter. Including the hadron-quark phase transition in the hypernuclear matter, we further study the mass-radius relation of hybrid stars. Results from different values of the symmetry energy parameter x, the bag constant, and attractive and repulsive ΣN interactions are compared.

A. Hypernuclear matter

Using the extended MDI interaction with hyperons (MDI-Hyp), we have studied the particle fractions in hypernuclear matter as functions of the baryon density. The results are shown in Fig. 6 for MDI-Hyp-A [(a) with $x=0$ and (b) with $x=-1$] and MDI-Hyp-R [(c) with $x=0$ and (d) with $x=-1$] interactions. The density dependence of corresponding particle chemical potentials is shown in Fig. 7. It is seen that the effect of hyperons is more pronounced at higher densities, and the appearance of hyperons prevents the neutron chemical potential from increasing too fast. Similar to the results from other works, the Λ hyperon appears at a baryon density of about $3\rho_0$. For the Σ hyperon, the density at which it appears depends on the sign of the ΣN interaction. For the attractive

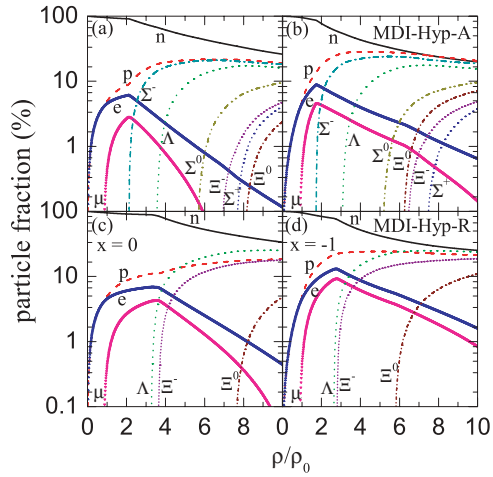

FIG. 6. (Color online) Particle fractions in hypernuclear matter for the MDI-Hyp interaction with $x=0$ [(a) and (c)] and $x=-1$ [(b) and (d)] as well as with attractive [(a) and (b)] and repulsive [(c) and (d)] ΣN interactions.

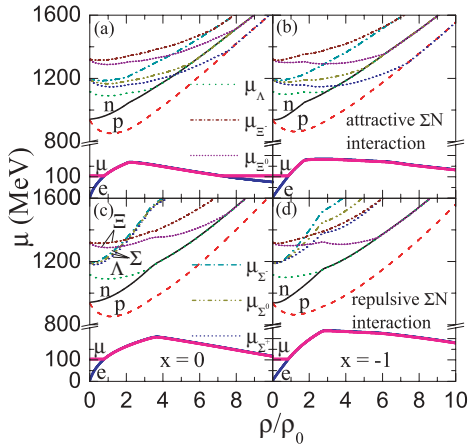

FIG. 7. (Color online) Same as Fig. 6 for the chemical potentials in hypernuclear matter.

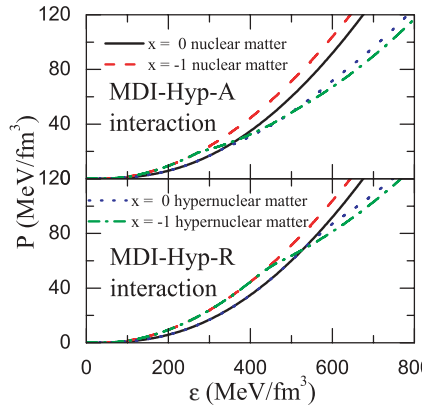

FIG. 8. (Color online) Equation of state of pure nuclear matter and hypernuclear matter from the MDI-Hyp interaction with $x = 0$ and $x = -1$ as well as with attractive (upper panel) and repulsive (lower panel) ΣN interactions.

MDI-Hyp-A interaction, it appears at about $2\rho_0$, whereas for the repulsive MDI-Hyp-R interaction, it does not appear until very high densities owing to the rapid increase of the chemical potentials of Σ hyperons with increasing total baryon density as shown in Fig. 7, making it difficult to satisfy the β-equilibrium condition at small baryon densities. This result is similar to that reported in the literature [31,40]. Also, with the value $x = -1$, corresponding to a stiffer symmetry energy, the fractions of leptons are lower at subsaturation densities but higher at higher densities, which results in a larger charge chemical potential at higher densities and the appearance of negatively (positively) charged hyperons at a lower (higher) density. A stiffer symmetry energy also increases the neutron chemical potential and thus leads to larger total hyperon fractions at higher densities. Since the total charge of the hypernuclear matter is conserved, an increase in the fraction of negatively charged hyperons results in an increasing fraction of protons and decreasing fraction of leptons. We note that for the MDI-Hyp-R interaction and at a density of $10\rho_0$, about 50% of the particle fraction is made up by hyperons, and the fraction of Λ particles is larger than that of protons at high densities.

In Fig. 8, we show the equation of state of nuclear matter from the MDI interaction with $x = 0$ and $x = -1$ and of hypernuclear matter from the MDI-Hyp-A and MDI-Hyp-R interactions. It is seen that the EOS is softened when hyperons are present as compared to the EOSs of pure nuclear matter. We note that the EOS at moderate densities plays an important role in determining the maximum mass of neutron stars. Without hyperons, the EOS at moderate densities is stiffer for smaller value of x, whereas it becomes stiffer for larger value of x when hyperons are included, especially for a repulsive ΣN interaction. As shown in Fig. 6, a stiffer symmetry energy leads to a larger number of hyperons, which results in a softer EOS as a result of the lower pressure owing to the presence of more degrees of freedom, and the effect of hyperons on the EOS is smaller for a soft symmetry energy, as fewer hyperons are then present in the hypernuclear matter. However, the symmetry energy contribution to the pressure of hypernuclear matter is larger for $x = -1$ than for $x = 0$. As a result, the EOS of hypernuclear matter shows similar stiffness for different symmetry energy parameters. Furthermore, the EOS from the MDI-Hyp-R interaction is stiffer than that from the MDI-Hyp-A interaction, as Σ particles do not appear in the former case as shown in Fig. 6. Our results thus show that hypernuclear matter has a stiffer (softer) EOS at lower densities but a softer (stiffer) EOS at moderate densities with a stiffer (softer) nuclear symmetry energy. We note that the results from both $x = 0$ and $x = -1$ are consistent with the constraints on the nuclear equation of state obtained from the analysis of the collective flow data in heavy-ion collisions [70].

B. The hadron-quark phase transition

At higher densities in the core of a neutron star, a transition from hadron matter to quark matter is expected to occur. Here we only consider the hadron-quark phase transition for the repulsive ΣN interaction as it is more consistent with the latest empirical information [56–60]. In Fig. 9, we display the particle fractions of each species in the presence of a hadron-quark phase transition, with the hadron phase from the MDI-Hyp-R interaction with $x = 0$ and $x = -1$ and the quark phase from the MIT bag model with bag constants $B^{1/4} = 180$ and 170 MeV. The particle fractions are weighted by the baryon number and corresponding phase fraction. It is seen that for $B^{1/4} = 180$ MeV, the phase transition begins at a density of 0.35 fm^{-3} and ends at a density of 1.38 fm^{-3} for $x = 0$, and it begins at a density of 0.26 fm^{-3} and ends at a density of 1.38 fm^{-3} for $x = -1$, whereas for $B^{1/4} = 170$ MeV it begins at a density of 0.21 fm^{-3} and ends at a density of 1.05 fm^{-3} for $x = 0$, and it begins at a density of 0.18 fm^{-3} and ends at a density of 1.05 fm^{-3} for $x = -1$. The hadron-quark phase transition thus happens at lower baryon number density for a stiffer symmetry energy and for a smaller value of B, whereas the density at which the hadron-quark phase transition ends seems to depend only on the value of B but not much on the value of the symmetry energy parameter x. With a smaller value of the bag constant, the hadron-quark phase transition both begins and ends earlier. It is also seen that d

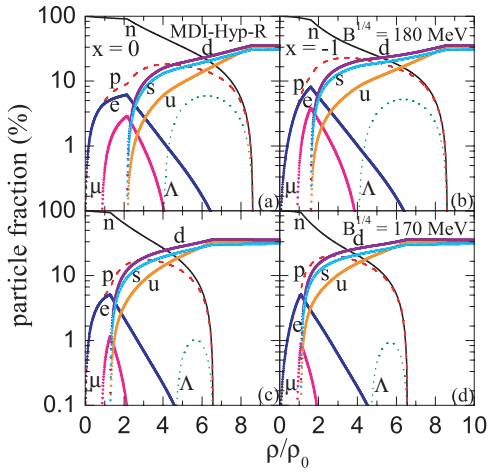

FIG. 9. (Color online) Particle fractions in hypernuclear matter with the presence of hadron-quark phase transition from the MDI-Hyp-R interaction with $x = 0$ [(a) and (c)] and $x = -1$ [(b) and (d)] for the hadron phase and the MIT bag model for the quark phase. Results from $B^{1/4} = 180$ MeV [(a) and (b)] and 170 MeV [(c) and (d)] are shown for comparison.

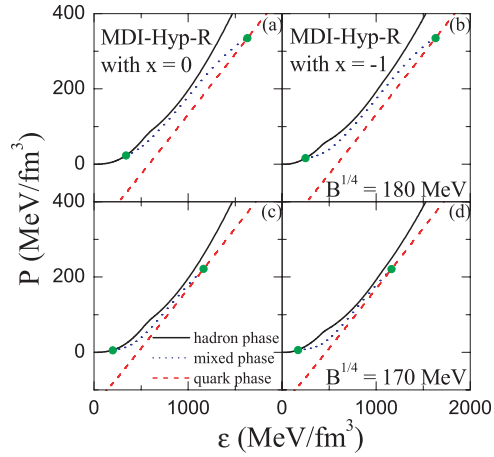

FIG. 10. (Color online) Same as Fig. 9 for the equation of state.

and s quarks occupy a larger fraction than u quarks in the mixed phase because of their negative charges, so the lepton fraction decreases while the proton fraction increases when the hadron-quark phase transition occurs. Furthermore, only Λ hyperons (i.e., no other hyperons) appear in the mixed phase in our model. The fraction of Λ hyperons is, however, sensitive to the value of the bag constant B, and with a smaller value of B its fraction becomes smaller.

The equations of state in the presence of the hadron-quark phase transition are shown in Fig. 10 with $B^{1/4} = 180$ and 170 MeV. Our results show that the equations of state of the mixed phase and the quark phase are both softened in comparison with a pure hadron phase. The difference between the results from $x = 0$ and $x = -1$ is not large except for the different starting density of the hadron-quark phase transition. Since the EOS is more sensitive to the value of bag constant than to the value of x when the quark degrees of freedom are introduced, the bag constant B is thus the main parameter in determining the EOS of dense matter, as reported in other work [22]. The energy density at the end of the hadron-quark phase transition is about 1.2 GeV/fm^3 for $B^{1/4} = 180$ MeV and about 1.6 GeV/fm^3 for $B^{1/4} = 170$ MeV, with the former closer to the value of about 1 GeV/fm^3 obtained from the lattice QCD calculation [71] and extracted from heavy-ion collision experiments [72]. Compared with the EOS constrained by the collective flow data in heavy-ion collisions [70], our results from both values of bag constants satisfy the empirical constraint.

C. Hybrid stars

In this section, we use the MDI-Hyp interaction to study the properties of static hybrid stars with spherically symmetric mass distributions. In particular, we calculate the mass-radius relation of a hybrid stars using the Tolman-Oppenheimer-Volkoff (TOV) equation [73,74]

$$\frac{dP}{dr} = -\frac{(\epsilon + P)(m_g + 4\pi r^3 P)}{r(r - 2m_g)}, \tag{30}$$

where m_g is the gravitational mass inside the radius r of the hybrid star given by

$$\frac{dm_g}{dr} = 4\pi r^2 \epsilon(r), \tag{31}$$

with $\epsilon(r)$ being the energy density. These equations are solved by starting from a central energy density $\epsilon(r = 0) \equiv \epsilon_c$ and integrating outward until the pressure on the surface of the hybrid star defined by $r = R$ vanishes [i.e, $P(R) = 0$]. This gives the radius R, and the total gravitational mass of a hybrid star is then given by $M = m_g(R)$.

In our calculations, the hybrid star is divided into three parts from the center to the surface: the liquid core, the inner crust, and the outer crust as in our previous work [12,13]. The liquid core is assumed to be of hypernuclear matter or with the hadron-quark phase transition, and the resulting equations of state shown in previous sections are used. In the inner crust, a parametrized EOS of $P = a + b\epsilon^{4/3}$ is used as in the previous treatment [12,13]. The outer crust usually consists of heavy nuclei and an electron gas, where we use the Baym, Pethick, and Sutherland EOS [75]. The transition density ρ_t between the liquid core and the inner crust has been consistently determined in our previous work [12,13], and for the density that distinguishes the edge of the inner crust and the outer crust, we take it to be $\rho_{\rm out} = 2.46 \times 10^{-4}$ fm^{-3}. The parameters a and b can then be determined by the pressures and energy densities at ρ_t and $\rho_{\rm out}$.

In Fig. 11, we show the mass-radius (M-R) and mass-central density (M-ρ_c) relations of hybrid stars from the EOS of hypernuclear matter without the hadron-quark phase transition as obtained here based on the MDI-Hyp interaction. Results using both attractive and repulsive ΣN interactions are shown, and the results from a pure nucleonic approach without hyperons are also shown for comparison. The maximum mass obtained with hyperons in hybrid stars is seen to be smaller as the EOS of the hypernuclear matter is softer than that of the nuclear matter. The equations of state at moderate densities

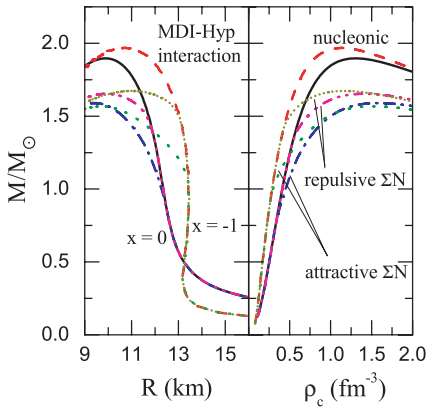

FIG. 11. (Color online) The hybrid star mass as a function of radius (left panel) and central density (right panel) based on the MDI-Hyp interaction with $x = 0$ and $x = -1$. Results from attractive and repulsive ΣN interactions are shown for comparison. Results from a pure nucleonic approach are also displayed.

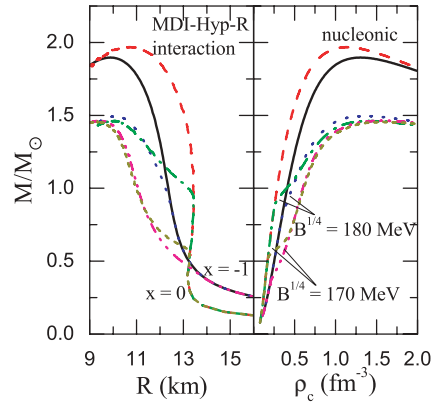

FIG. 12. (Color online) The hybrid star mass as a function of radius (left panel) and central density (right panel) in the presence of the hadron-quark phase transition. Results from the MDI-Hyp-R interaction for the hadron phase with $x = 0$ and $x = -1$ and the MIT bag model for the quark phase with $B^{1/4} = 180$ and 170 MeV are shown for comparison. Results from a pure nucleonic approach are also displayed.

play an important role in determining the maximum mass, as the M-ρ_c relation shows that the neutron star mass cannot increase even when the central density reaches a very high value. The mass is larger when a repulsive ΣN interaction is used as a result of the smaller number of degrees of freedom and stiffer EOS, as discussed in the previous section. For smaller values of ρ_c a stiffer symmetry energy gives a larger mass as the nuclear matter dominates this density range, and the results are thus the same as those in our previous work [12,13]. With larger ρ_c, the effect due to the nuclear symmetry energy is small, and the mass from $x = 0$ is similar to that from $x = -1$ because of the opposing effects from the symmetry pressure and the fraction of hyperons on the equation of state. The maximum mass obtained with an attractive ΣN interaction is $1.59M_\odot$ for $x = 0$ and $1.57M_\odot$ for $x = -1$, where $M_\odot$ is the solar mass. With a repulsive ΣN interaction the maximum mass increases to $1.65M_\odot$ for $x = 0$ and $1.67M_\odot$ for $x = -1$. Our results thus differ from those of many previous works [38,39] that limit the maximum mass of hybrid stars from reaching the canonical value of $1.4M_\odot$. In our model, the radius of a hybrid star with a mass of $1.4M_\odot$ is 11.2 km for $x = 0$ and 11.9 km for $x = -1$ for an attractive ΣN interaction and 11.9 km for $x = 0$ and 13.2 km for $x = -1$ for a repulsive ΣN interaction, respectively.

In Fig. 12, the M-R and M-ρ_c relations are displayed for hybrid stars with the hadron-quark phase transition in their liquid core. Again, results from the hadron phase with $x = 0$ and $x = -1$ and the quark phase with $B^{1/4} = 180$ MeV and $B^{1/4} = 170$ MeV are shown, and those from a pure nucleonic approach are also shown for comparison. The maximum mass for $B^{1/4} = 180$ MeV is $1.50M_\odot$ for $x = 0$ and $1.46M_\odot$ for $x = -1$, and for $B^{1/4} = 170$ MeV it is $1.46M_\odot$ for $x = 0$ and $1.45M_\odot$ for $x = -1$, respectively. The radius of a standard neutron star with a mass of $1.4M_\odot$ is 11.0 km for $x = 0$ and 10.8 km for $x = -1$ for $B^{1/4} = 180$ MeV and 10.2 km for $x = 0$ and 10.0 km for $x = -1$ for $B^{1/4} = 170$ MeV. If we further reduce the value of B, the hadron-quark phase transition would happen at an even lower density, and the maximum mass for the hybrid star would correspond to a larger central density and a smaller radius. These results are obtained with the Gibbs construction for the hadron-quark phase transition. With the Maxwell construction, the radius of a maximum-mass hybrid star would be larger. Within our model, both treatments of the phase transition give, however, reasonable masses and radii for hybrid stars.

Finally, we note that the original MDI interaction does not lead to the violation of causality in β-stable $npe\mu$ matter up to $10\rho_0$ as shown in Fig. 2(d) in Ref. [13]. Since the EOS of neutron star matter is softened by the presence of hyperons and quarks, the causality condition is still satisfied for the extended MDI interaction used in the present study, and this is confirmed by explicit calculations.

V. SUMMARY

We have extended the MDI interaction for the nucleon-nucleon effective interaction in the nuclear medium to include the nucleon-hyperon and hyperon-hyperon interactions by assuming that they have the same density and momentum dependence as that for the nucleon-nucleon interaction. The parameters were determined by fitting the empirical hyperon single-particle potentials in symmetric nuclear matter at its saturation density. As an example for the application of the extended MDI interaction, we investigated the properties of hybrid stars that include not only the hyperon degree of freedom but also that of quarks by taking into account the phase transition between the hadron and quark phases. Our results indicate that the extended MDI interaction can give a reasonable description of the hypernuclear matter. We found that the EOS of the hypernuclear matter is much softer than that of pure nuclear matter and that it becomes even softer if the hadron-quark phase transition is included. The masses and radii of hybrid stars were also studied with these equations of state, and they were found to remain reasonable after including hyperons and the hadron-quark phase transition. We have also studied the effects of attractive and repulsive ΣN interactions and different symmetry energies on the hybrid

star properties. The results show that the appearance of the Σ hyperon in hybrid stars depends sensitively on the sign of the ΣN interaction with a repulsive ΣN interaction giving a higher critical density for the appearance of Σ hyperons. In addition, a stiffer symmetry energy usually leads to a larger fraction of hyperons in the hypernuclear matter. We further found that both the low-density boundary of the hadron-quark phase transition and the EOS at high densities in hybrid stars are more sensitive to the bag constant than to the stiffness of the nuclear symmetry energy at high densities. This extended MDI interaction, which gives isospin- and momentum-dependent in-medium effective interactions for the baryon octet, will also be very useful in transport models that simulate heavy-ion reactions in future radioactive beam facilities, particularly at the FAIR/GSI energies.

ACKNOWLEDGMENTS

We thank David Blaschke for critical comments on an earlier version of this paper. This work was supported in part by the US National Science Foundation under Grant Nos. PHY-0758115, PHY-0652548, and PHY-0757839, the Welch Foundation under Grant No. A-1358, the Research Corporation under Grant No. 7123, the Texas Coordinating Board of Higher Education Grant No. 003565-0004-2007, the National Natural Science Foundation of China under Grant Nos. 10675082 and 10975097, the MOE of China under Project No. NCET-05-0392, Shanghai Rising-Star Program under Grant No. 06QA14024, the SRF for ROCS, SEM of China, and the National Basic Research Program of China (973 Program) under Contract No. 2007CB815004.

[1] C. B. Das, S. Das Gupta, C. Gale, and B. A. Li, Phys. Rev. C **67**, 034611 (2003).
[2] B. A. Li, L. W. Chen, and C. M. Ko, Phys. Rep. **464**, 113 (2008).
[3] M. B. Tsang *et al.*, Phys. Rev. Lett. **92**, 062701 (2004).
[4] L. W. Chen, C. M. Ko, and B. A. Li, Phys. Rev. Lett. **94**, 032701 (2005).
[5] B. A. Li and L. W. Chen, Phys. Rev. C **72**, 064611 (2005).
[6] L. W. Chen, C. M. Ko, and B. A. Li, Phys. Rev. C **72**, 064309 (2005).
[7] B. A. Li and A. Steiner, Phys. Lett. B **642**, 436 (2006).
[8] P. G. Krastev, B. A. Li, and A. Worley, Astrophys. J. **676**, 1170 (2008).
[9] P. G. Krastev, B. A. Li, and A. Worley, Phys. Lett. B **668**, 1 (2008).
[10] D. H. Wen, B. A. Li, and P. G. Krastev, Phys. Rev. C **80**, 025801 (2009).
[11] W. G. Newton and B. A. Li, Phys. Rev. C **80**, 065809 (2009).
[12] J. Xu, L. W. Chen, B. A. Li, and H. R. Ma, Phys. Rev. C **79**, 035802 (2009).
[13] J. Xu, L. W. Chen, B. A. Li, and H. R. Ma, Astrophys. J. **697**, 1549 (2009).
[14] N. Itoh, Prog. Theor. Phys. **44**, 291 (1970).
[15] J. C. Collins and M. J. Perry, Phys. Rev. Lett. **34**, 1353 (1975).
[16] U. Heinz, P. R. Subramanian, H. Stocker, and W. Greiner, J. Phys. G **12**, 1237 (1986).
[17] G. F. Burgio, M. Baldo, P. K. Sahu, and H. J. Schulze, Phys. Rev. C **66**, 025802 (2002).
[18] G. F. Burgio, M. Baldo, P. K. Sahu, A. B. Santra, and H. J. Schulze, Phys. Lett. B **526**, 19 (2002).
[19] C. Maieron, M. Baldo, G. F. Burgio, and H. J. Schulze, Phys. Rev. D **70**, 043010 (2004).
[20] M. Di Toro, A. Drago, T. Gaitanos, V. Greco, and A. Lavagno, Nucl. Phys. A **775**, 102 (2006).
[21] G. H. Bordbar, M. Bigdeli, and T. Yazdizadeh, Int. J. Mod. Phys. A **21**, 5991 (2006).
[22] N. N. Pan and X. P. Zheng, Chin. J. Astron. Astrophys. **7**, 675 (2007).
[23] D. B. Blaschke, D. Gómez Dumm, A. G. Grunfeld, T. Klahn, and N. N. Scoccola, Phys. Rev. C **75**, 065804 (2007).
[24] J. D. Carroll, D. B. Leinweber, A. G. Williams, and A. W. Thomas, Phys. Rev. C **79**, 045810 (2009).
[25] F. Yang and H. Shen, Phys. Rev. C **77**, 025801 (2008).
[26] G. X. Peng, A. Li, and U. Lombardo, Phys. Rev. C **77**, 065807 (2008).
[27] N. K. Glendenning, Phys. Rev. D **46**, 1274 (1992).
[28] N. K. Glendenning, Phys. Rep. **342**, 393 (2001).
[29] A. Chodos, R. L. Jaffe, K. Johnson, C. B. Thorn, and V. F. Weisskopf, Phys. Rev. D **9**, 3471 (1974).
[30] J. Schaffner, C. B. Dover, A. Gal, C. Greiner, and H. Stocker, Phys. Rev. Lett. **71**, 1328 (1993).
[31] J. Schaffner and I. N. Mishustin, Phys. Rev. C **53**, 1416 (1996).
[32] J. Schaffner-Bielich and A. Gal, Phys. Rev. C **62**, 034311 (2000).
[33] M. H. Weng, X. H. Guo, and B. Liu, arXiv:0910.5334v1 [hep-ph].
[34] G. Y. Shao and Y. X. Liu, Phys. Rev. C **79**, 025804 (2009).
[35] H. J. Schulze, A. Lejeune, J. Cugnon, M. Baldo, and U. Lombardo, Phys. Lett. B **355**, 21 (1995).
[36] H. J. Schulze, M. Baldo, U. Lombardo, J. Cugnon, and A. Lejeune, Phys. Rev. C **57**, 704 (1998).
[37] M. Baldo, G. F. Burgio, and H. J. Schulze, Phys. Rev. C **58**, 3688 (1998).
[38] M. Baldo, G. F. Burgio, and H. J. Schulze, Phys. Rev. C **61**, 055801 (2000).
[39] I. Vidaña, A. Polls, A. Ramos, L. Engvik, and M. Hjorth-Jensen, Phys. Rev. C **62**, 035801 (2000).
[40] S. Balberg and A. Gal, Nucl. Phys. A **625**, 435 (1997).
[41] S. Banik and D. bandyopadhyay, J. Phys. G **26**, 1495 (2000).
[42] M. B. Tsang, Y. Zhang, P. Danielewicz, M. Famiano, Z. Li, W. G. Lynch, and A. W. Steiner, Phys. Rev. Lett. **102**, 122701 (2009).
[43] This convention is different from that of Ref. [2], which uses $\tau_N = 1/2$ for neutrons and $\tau_N = -1/2$ for protons.
[44] O. Hashimoto and H. Tamura, Prog. Part. Nucl. Phys. **57**, 564 (2006).
[45] C. B. Dover, D. J. Millener, and A. Gal, Phys. Rep. **184**, 1 (1989).
[46] S. Bart *et al.*, Phys. Rev. Lett. **83**, 5238 (1999).
[47] C. B. Dover and A. Gal, Ann. Phys. **146**, 309 (1983).
[48] P. M. M. Maessen, Th. A. Rijken, and J. J. de Swart, Phys. Rev. C **40**, 2226 (1989).
[49] J. Dabrowski, Phys. Rev. C **60**, 025205 (1999).
[50] A. Reuber, K. Holinda, and J. Speth, Nucl. Phys. A **570**, 543 (1994).
[51] D. J. Millener, C. B. Dover, and A. Gal, Phys. Rev. C **38**, 2700 (1988).

[52] R. E. Chrien and C. B. Dover, Annu. Rev. Nucl. Part. Sci. **39**, 113 (1989).
[53] S. Aoki *et al.*, Phys. Lett. B **355**, 45 (1995).
[54] T. Fukuda *et al.*, Phys. Rev. C **58**, 1306 (1998).
[55] P. Khaustov *et al.*, Phys. Rev. C **61**, 054603 (2000).
[56] J. Mareš, E. Friedman, A. Gal, and B. K. Jennings, Nucl. Phys. A **594**, 311 (1995).
[57] E. Friedman and A. Gal, Phys. Rep. **452**, 89 (2007).
[58] C. J. Batty, E. Friedman, and A. Gal, Phys. Lett. B **335**, 273 (1994).
[59] H. Noumi *et al.*, Phys. Rev. Lett. **89**, 072301 (2002).
[60] T. Harada and Y. Hirabayashi, Nucl. Phys. A **759**, 143 (2005).
[61] J. Schaffner, C. B. Dover, A. Gal, M. Hanauske, C. Greiner, D. J. Millener, and H. Stöcker, Ann. Phys. **235**, 35 (1994).
[62] H. Dapo, B. J. Schaefer, and J. Wambach, arXiv:0811.2939v3 [nucl-th].
[63] H. Polinder, J. Haidenbauer, and U. G. Meißner, Nucl. Phys. A **779**, 244 (2006).
[64] S. Hama, B. C. Clark, E. D. Cooper, H. S. Sherif, and R. L. Mercer, Phys. Rev. C **41**, 2737 (1990).
[65] E. D. Cooper, S. Hama, B. C. Clark, and R. L. Mercer, Phys. Rev. C **47**, 297 (1993).
[66] Q. Li, Z. Li, E. Zhao, and R. K. Gupta, Phys. Rev. C **71**, 054907 (2005).
[67] A. Bhattacharyya, I. N. Mishustin, and W. Greiner, J. Phys. G **37**, 025201 (2010).
[68] H. Heiselberg, C. J. Pethick, and E. F. Staubo, Phys. Rev. Lett. **70**, 1355 (1993).
[69] T. Maruyama *et al.*, Phys. Lett. B **659**, 192 (2008).
[70] P. Danielewicz, R. Lacey, and W. G. Lynch, Science **298**, 1592 (2002).
[71] M. Cheng *et al.*, Phys. Rev. D **81**, 054504 (2010).
[72] U. Heinz and M. Jacobs, arXiv:nucl-th/0002042v1; U. Heinz, Nucl. Phys. A **685**, 414 (2001).
[73] J. Oppenheimet and G. Volkoff, Phys. Rev. **55**, 374 (1939).
[74] I. A. Morrison, T. W. Baumgarte, S. L. Shapiro, and V. R. Pandharipande, Astrophys. J. **617**, L135 (2004).
[75] G. Baym, C. Pethick, and P. Sutherland, Astrophys. J. **170**, 299 (1971).